Journal of Power Sources 195 (2010) 1015–1023

Contents lists available at ScienceDirect

Journal of Power Sources

journal homepage: www.elsevier.com/locate/jpowsour

# Simultaneously enhanced methanol barrier and proton conductive properties of phosphorylated titanate nanotubes embedded nanocomposite membranes

Jingtao Wang, Yuning Zhao, Weiqiang Hou, Jiaqing Geng, Lulu Xiao, Hong Wu, Zhongyi Jiang*

*Key Laboratory for Green Chemical Technology, School of Chemical Engineering and Technology, Tianjin University, 92# Weijin Road, Nankai District, Tianjin 300072, China*

ARTICLE INFO

*Article history:*
Received 6 June 2009
Accepted 19 August 2009
Available online 27 August 2009

*Keywords:*
Phosphorylated titanate nanotubes
Chitosan
Nanocomposite membrane
Direct methanol fuel cell
Methanol permeability
Proton conductivity

ABSTRACT

The current study aims at simultaneously enhancing the methanol barrier and proton conductive properties of membranes for direct methanol fuel cell (DMFC) by embedding phosphorylated titanate nanotubes (PTNTs) into chitosan (CS) membrane. The enhancement is most probably due to the intrinsic interfacial interactions between PTNTs and CS chains, which are verified by the increased thermal stability and homogeneous dispersion of the fillers. The influence of PTNTs incorporation conditions including acid concentration and filler content upon the resulting nanocomposite membrane performance is extensively investigated. Compared with plain CS membrane, the presence of PTNTs within chitosan matrix will lead to denser chain packing, thus reduce free volume cavity size and fractional free volume (*FFV*) according to positron annihilation lifetime spectroscopy analysis. The reduced *FFV* and more tortuous pathway significantly suppress the methanol crossover through the membranes. Meanwhile, the presence of PTNTs constructs an uninterrupted channel for proton migration via functionalized P–OH groups and adsorbed water, and therefore improving the proton conductivity substantially. As a result, the nanocomposite membranes exhibit desirable comprehensive performance, which is about ten times higher than that of Nafion 117. We envisage that the current observations hint the encouraging application promises of such nanocomposite membranes in DMFC.



## 1. Introduction

Direct methanol fuel cell (DMFC) is a strong candidate for new portable power devices (e.g. future laptop computers and cell phones) and has attracted burgeoning interest in the last few years [1–3]. One of the important challenges in the current DMFC research is to develop an alternative proton exchange membrane (PEM) to the perfluorinated ionomers, for example, Nafion (Du pont). At low temperatures and high levels of hydration, these membranes exhibited high proton conductivities (in the range of $10^{-2}$–$10^{-1}$ S cm$^{-1}$) owing to their ion-cluster channels formed by hydrophilic sulfonated side chains for proton continuous migration [4,5]. Nevertheless, these channels also caused considerable membrane swelling and serious methanol crossover from anode to cathode, which reduced the open-circuit potential by as much as 0.15–0.2 V and poisoned the electrocatalysts at the cathode [6].

To address these issues, significant contributions have been dedicated to constructing new proton transport pathways by embedding proton conductive inorganic materials into polymer matrix which could effectively facilitate proton conductivity as well as inhibit methanol crossover by blocking methanol transport path and/or suppressing membrane swelling [7–10]. Among various inorganic materials, nanotubes have currently triggered increasing attention as reinforcing materials for polymers due to their high aspect ratios which allowed to form an uninterrupted trajectory for proton transport [11–13]. Thomassin et al. [12] prepared carboxylic acid grafted carbon nanotubes, and noticed an enhancement of proton conductivity by approximate 5% of the nanotubes impregnated Nafion membrane compared with bare Nafion membrane at room temperature. Notable enhancement in proton conductivity was obtained by sulfonic acid functionalized nanotubes. Joo et al. [13] developed a sulfonated carbon nanotubes–Nafion composite membrane, which possessed higher proton conductivity (by about 20%) than that of plain Nafion membrane at constant temperature.

Compared with sulfonic acid groups, phosphoric acid groups possessed lower average zero point energy (37.2 kJ mol$^{-1}$ for phosphoric acid vs. 69.9 kJ mol$^{-1}$ for sulfonic acid) and higher water binding energy (47.3 kJ mol$^{-1}$ for phosphoric acid vs. 44.4 kJ mol$^{-1}$ for sulfonic acid), and hence displayed lower proton migration barrier and higher water retention properties [14]. Especially under intermediate temperature and low relative humidity even anhydrous conditions, phosphoric acid-bearing membranes exhibited superior proton conductivity to sulfonic acid by Grotthuss mechanism [15,16]. Based on these findings, phosphoric acid modification of polymers or inorganic fillers has been widely uti-

* Corresponding author. Tel.: +86 22 23500086; fax: +86 22 23500086.
*E-mail address:* zhyjiang@tju.edu.cn (Z. Jiang).

0378-7753/$ – see front matter © 2009 Elsevier B.V. All rights reserved.
doi:10.1016/j.jpowsour.2009.08.053

lized to improve the proton conductivity of the PEM in recent years [17–22]. Compared with the phosphorylation of polymers, chemical modification of inorganic fillers by phosphoric acid has been demonstrated as an effective, generic, facile approach to introduce acidic groups [23]. Spherical phosphorylated particles were widely employed to enhance the proton conductivity of the composite membranes [19,20]. In particular, the incorporation of zirconium tricarboxybutylphosphonate into polybenzimidazole significantly improved the proton conductivity by more than one order of magnitude compared with plain polybenzimidazole membrane [19]. Sheet phosphorylated materials were already used as fillers of composite proton exchange membrane [21,22]. Under the optimum conditions, the proton conductivity of these membranes could be increased up to $10^{-1}$ S cm$^{-1}$. However, despite the numerous investigations on spherical and sheet phosphorylated materials, tubular phosphorylated materials have seldom been reported as additives for composite membrane fabrication.

In this work, we described for the first time the use of phosphorylated nanotubes as inorganic fillers to enhance the membrane performance for DMFC application. Phosphorylated titanate nanotubes (PTNTs) of varying phosphoric acid contents were synthesized and then impregnated into polymer matrix to fabricate nanocomposite membranes. The objective of this study was to simultaneously enhance methanol barrier and proton conductive properties of the membranes. The essence of our discovery was mainly embodied in the following experiments: systematically examine the effect of PTNTs on the membrane performance including water uptake, swelling, methanol permeability and proton conductivity. Moreover, the physiochemical properties of the membranes in terms of chemical structure, thermal stability, morphology and free volume characteristics were investigated in detail.

## 2. Experimental

### 2.1. Materials and chemicals

Rutile-type titanium dioxide powders were purchased from Shanghai Zhuerna High-tech Powder Material Co., Ltd., and used without further purification. Chitosan (CS) with a degree of deacetylation of 91% was purchased from Golden-Shell Biochemical Co. (Zhejiang, China) and used as received. Acetic acid, sulfuric acid and methanol were of analytical grade and supplied from Tianjin. Phosphoric acid, sodium dihydrogen phosphate, disodium hydrogen phosphate and sodium phosphate were commercially available as analytical grade and used without any further purification. Deionized water was used in all experiments.

### 2.2. Preparation of phosphorylated titanate nanotubes

Titanate nanotubes (TNTs) were synthesized by a hydrothermal method as described by Geng et al. [24]. The titanate nanotubes were phosphorylated by chemical absorption according to the procedure in the literatures [25,26]. The TNTs were immersed into 0.5 M phosphoric acid solution under stirring for a certain time (3, 6, 9 or 12 h) at 20 ± 2 °C. Thereafter, the resulting suspension mixture was filtrated to separate the precipitates, which were then washed with de-ionized water repeatedly till the pH value of washing solution reached 7.0 so that the free phosphoric acid was completely eluted. The phosphorylated titanate nanotubes were obtained after drying at 60 °C in oven overnight. These phosphorylated tubes were designated as PTNT-3 h, PTNT-6 h, PTNT-9 h and PTNT-12 h, corresponding to the immersing time.

The PTNTs modified by different phosphorylation reagents were fabricated via the similar procedure. The TNTs were immersed in four different solutions including $H_3PO_4$ (0.5 M, pH 1.7), $NaH_2PO_4$ (0.5 M, pH 4.7), $Na_2HPO_4$ (0.5 M, pH 9.2) and $Na_3PO_4$ (0.5 M, pH 13.2) for 6 h. Different from the sample modified by $H_3PO_4$, before being washed with de-ionized water, the other three samples were dispersed and immersed in 0.1 M HCl solution for 2 h, followed by being washed with 0.1 M HCl solution repeatedly to exchange $Na^+$ in tubes with $H^+$. For simplicity, the resulting PTNTs were designated as PTNT-H3, PTNT-H2, PTNT-H1 and PTNT-H0, corresponding to $H_3PO_4$, $NaH_2PO_4$, $Na_2HPO_4$ and $Na_3PO_4$ as the phosphorylation reagents.

### 2.3. Preparation of CS/PTNT nanocomposite membranes

Chitosan (1.5 g) was dissolved in 40 mL of 2 wt% acetic acid aqueous solution under stirring at 80 °C. Simultaneously, PTNTs (0.225 g, 15 wt% corresponding to chitosan) were dispersed into 35 mL of 2 wt% acetic acid aqueous solution with ultrasonic treatment for 30 min. These two parts of solution were then mixed and stirred vigorously at 80 °C for another 2 h. After degasification, the resulting homogenous solution was cast onto a clear glass plate and dried at 25 °C. The membrane was afterwards immersed and cross-linked in 2 M $H_2SO_4$ for 24 h and then extensively rinsed with de-ionized water to remove residual $H_2SO_4$. Finally the nanocomposite membrane was dried under vacuum at 25 °C for 24 h. The resulting membranes were designated as CS/A, where A (A = PTNT-3 h, PTNT-H3, etc.) represented the fillers.

The nanocomposite membranes with different filler contents were fabricated in the similar procedure. Different amounts of PTNT-6 h were embedded into bulk chitosan, and the obtained membranes were designated as CS/PTNT-*X*, where *X* (*X* = 5, 10, 15, 20, 25 or 30) was the weight ratio of the tubes to chitosan.

### 2.4. Characterization

The morphology of the phosphorylated nanotubes was characterized by transmission electron microscopy (TEM, Tecnai G2 20 S-TWIN). The cross section of the membranes was observed using field emission scanning electron microscope (FESEM, Nanosem 430) operated at 5 kV after being freeze-fractured in liquid nitrogen and then sputtered with gold.

The elemental composition of the nanotubes was characterized by X-ray photoelectron spectroscopy (XPS) using a PHI 1600 spectrometer with an Mg Kα radiation for excitation. The Brunauer–Emmett–Teller (BET) surface area and pore volume of the powder sample were determined by nitrogen adsorption on an ASAP 2020 nitrogen adsorption apparatus.

Fourier transform infrared spectra (FTIR, 4000–400 cm$^{-1}$) of the tubes and membranes were recorded on a Nicolet MAGNA-IR 560 instrument. The thermogravimetric analysis (TGA, PerkinElmer Pyris) data of the membranes were obtained from 20 to 700 °C using a heating rate of 10 °C min$^{-1}$ at air atmosphere.

Positron annihilation lifetime spectroscopy (PALS) experiment was performed by using an EG&GORTEC fast–fast coincidence system (resolution, 201 ps) at room temperature. The resource of $^{22}$Na ($5 \times 10^5$ Bq) was sandwiched between two pieces of sample, each of which with an overall thickness of about 1.0 mm. The integral statistics for each spectrum was more than $2 \times 10^6$ coincidences. In this technique, assuming that o-Ps was localized in a spherical potential well surrounded by an electron layer of thickness $\Delta r$ equal to 0.1656 nm, the radius of free volume cavity ($r$) is obtained from pick-off annihilation lifetime ($\tau$) of o-Ps in the free volume elements by a semiempirical equation [27,28]:

$$\tau = \frac{1}{2}\left[1 - \frac{\gamma}{\gamma + \Delta\gamma} + \frac{1}{2\pi}\sin\left(\frac{2\pi\gamma}{\gamma + \Delta\gamma}\right)\right]^{-1} \quad (1)$$

The volume of the equivalent sphere can be calculated by Eq. (2):

$$V_f = \frac{4\pi}{3}\gamma^3 \quad (2)$$

Further, the fractional free volume (*FFV*) may be estimated from Eq. (3):

$$FFV = V_{f3}I_3 \quad (3)$$

where $V_f$ and $I$ are free volume of the sphere and intensity of o-Ps, respectively.

### 2.5. Water uptake and swelling

The water uptake of the membranes was determined as follows. The dry membrane was weighed ($W_{dry}$) and immersed in de-ionized water for 24 h at room temperature. Then the membrane was re-weighed ($W_{wet}$) quickly after removing the surface water. The surface swelling was determined in a similar method, by soaking the dry rectangular membrane (about 4.0 cm × 4.0 cm) with the area of $A_{dry}$ in de-ionized water for 24 h, then re-measuring to obtain the wetted membrane area ($A_{wet}$). The final values of water uptake and swelling were the average of the three measurements with an error within ±5.0% and calculated by Eqs. (4) and (5), respectively:

$$\text{water uptake}\,(\%) = \frac{W_{wet} - W_{dry}}{W_{dry}} \times 100 \quad (4)$$

$$\text{swelling}\,(\%) = \frac{A_{wet} - A_{dry}}{A_{dry}} \times 100 \quad (5)$$

### 2.6. Methanol permeability

The methanol permeability was measured with a glass diffusion cell as described in the literature [29], which consisted of two compartments with identical volume separated by a membrane sheet. The membrane was hydrated in de-ionized water for 24 h before being clamped tightly between the two compartments, one of which was initially filled with water and the other filled with 2.0 M methanol solution. The methanol concentration in the receipt compartment was determined using a gas chromatography (Agilent 6820) equipped with a TCD detector and a DB624 column. The methanol permeability ($P$, $cm^2\ s^{-1}$) was calculated from Eq. (6):

$$P = S\frac{V_B l}{AC_{A0}} \quad (6)$$

where $S$ is the slope of the straight line of concentration versus time, $V_B$ is the volume of the receipt compartment, $l$, $A$, and $C_{A0}$ are the membrane thickness, effective membrane area, and feed concentration, respectively. The measurement error was within ±4.0%.

### 2.7. Proton conductivity

The proton conductivity of the membranes in the horizontal direction was measured in two-point-probe conductivity cells by the AC impedance spectroscopy method. The membrane impedance was measured with a frequency response analyzer (FRA, Compactstat, IVIUM Tech.) over a frequency range of 1–$10^6$ Hz with oscillating voltage of 20 mV. The test temperature was controlled by the water vapor from room temperature to 80 °C. All the membrane samples were immersed in de-ionized for 48 h prior to the measurement. The proton conductivity ($\sigma$, $S\,cm^{-1}$) of the sample in transverse direction was calculated by Eq. (7):

$$\sigma = \frac{l}{AR} \quad (7)$$

where $l$ is the distance between the two probes, $A$ is the cross-sectional area of testing sample, and $R$ is the membrane resistance obtained from the FRA.

## 3. Results and discussion

### 3.1. Characterization of phosphorylated titanate nanotubes

Phosphoric acid is known to be adsorbed strongly on the surface of $TiO_2$ by chemical adsorption [25,30,31]. Phosphorylated $TiO_2$ materials are reported to be very stable over a wide pH range values, mainly due to Coulombic interaction [30]. The chemical structure of PTNTs was determined by FTIR and XPS. For titanate nanotubes, the FTIR spectrum in Fig. 1a had a strong peak at around 498 $cm^{-1}$ corresponding to the stretching vibration of Ti–O together with the peaks at 1635 and 3384 $cm^{-1}$ assigning to the deformation and stretching vibration of the adsorbed water. The introduction of phosphoric acid groups on the tube segments was verified by the appearance of the new sharp peak at 1045 $cm^{-1}$ that attributed to the stretching vibration of the P–OH [32]. Meanwhile, due to the high water retention ability of phosphoric acid groups, the intensity of the two characteristic peaks of water became stronger after the phosphorylation, which may facilitate the proton transport. XPS analysis was employed to examine the oxidation state and content of P on the $TiO_2$ surface. As shown in Fig. 1b, the XPS spectrum of pure TNTs exhibited the peak of binding energy at 462.5 eV corresponding to the Ti 2p. After the phosphorylation, the PTNTs exhibited a binding energy of P 2p located at around 134.0 eV, indicating that the P in our samples was in pentavalent-oxidation state ($P^{5+}$) and presented in the form of P–O bond [31]. The O 1s spectrum at 532.7 eV for TNTs (the lower in Fig. 1c) was corresponding to the Ti–O–Ti state. While this peak for PTNTs moved to 533.6 eV (the upper in Fig. 1c), which was related to oxygen in the P=O and Ti–O–P environments [26].

The microstructure of the PTNTs was determined by TEM and BET analysis as shown in Fig. 1d and e, respectively. TEM image demonstrated that homogenous phosphorylated titanate nanotubes with 11 nm tube diameter and 200–500 nm tube length were prepared. Fig. 1e shows the nitrogen adsorption–desorption isotherm of PTNTs, which indicated a hysteresis loop characteristic of open end mesoporous structures. BET results implied that the inner diameter with narrow size distribution of PTNTs was around 6.2 nm (Fig. 1e, inset). The PTNTs possessed typically large BET surface area about 264 $cm^2\ g^{-1}$, which might render high water retention ability. Collectively, these data confirmed that the PTNTs with 6.2 nm inner diameter, 200–500 nm tube length and large surface area were successfully prepared, which endowed the possibility to tailor the membrane performance by embedding these PTNTs into polymer matrix.

### 3.2. Characterization of CS/PTNT membranes

The influence of the PTNTs on physicochemical properties of the membranes was investigated using FTIR and TGA as shown in Figs. 2 and 3, respectively. FTIR spectra have been utilized to gain a better understanding of the interfacial interaction between the nanotubes and CS chains. According to the spectra, the major vibrational fingerprints associated with the CS membrane could be found in all the samples. O–H stretching vibrations could be observed at 3256 $cm^{-1}$, and the peaks at 1637 and 1535 $cm^{-1}$ arose from the vibration of amide I band and amide II band, respectively. After PTNTs incorporation, the absorption intensities of the three characteristic peaks became weaker (Fig. 2b–d). These observations indicated that the interfacial interactions including hydrogen-bonding and electrostatic interactions between chitosan

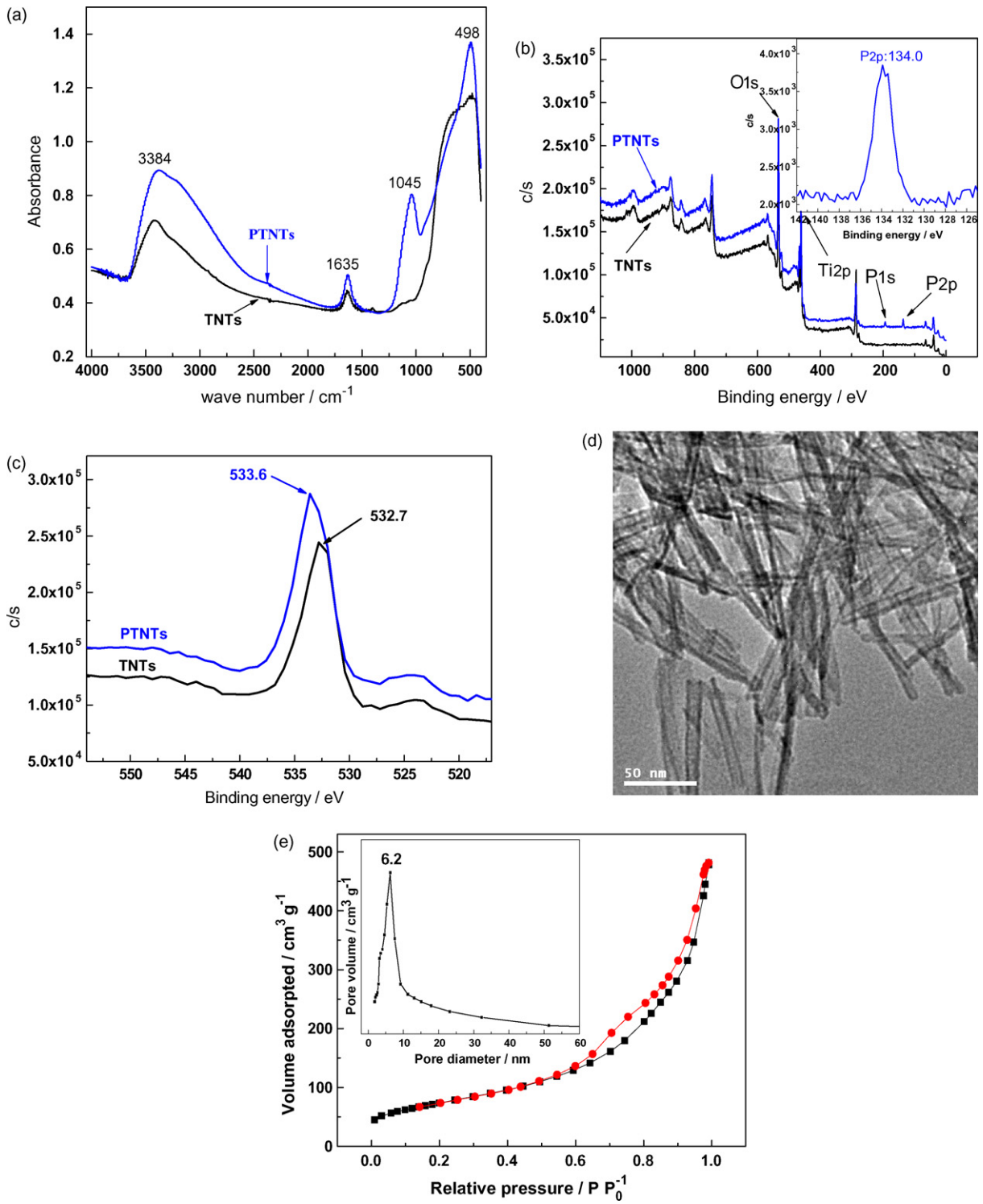


**Fig. 1.** Characterization of PTNTs: (a) FTIR spectra, (b and c) XPS spectra of P 2p and O 1s, (d) TEM image and (e) $N_2$ adsorption–desorption isotherm and BJH pore size distribution (inset).

and the additives were formed, which reduced the amounts of free hydroxy and amide groups of chitosan. Since more interactions were formed with the filler content, the intensities of these peaks decreased further (from Fig. 2b–d).

Thermal stability of CS/PTNT samples could be referred from their TGA thermograms (Fig. 3). In consistence with the results in the literature [33], all the membranes exhibited three-step weight loss character, comprising of water evaporation (loose and bound) from the membrane phase (step I, around 50–100 °C), degradation of chitosan chains (step II, around 220–310 °C), and final membrane matrix degradation (step III, around 480–650 °C). After the addition of PTNTs, an enhancement on thermal stability (steps II and III) and a retardation on the oxidative degradation were observed for these CS/PTNT samples. The enhancement was reasonably owing to the strong interactions at organic–inorganic interface, which inhibited the mobility of CS chains and therefore suppressed the decomposition of CS molecules. High filler content of the nanocomposite membranes resulted in high char yields at 700 °C. It was note-

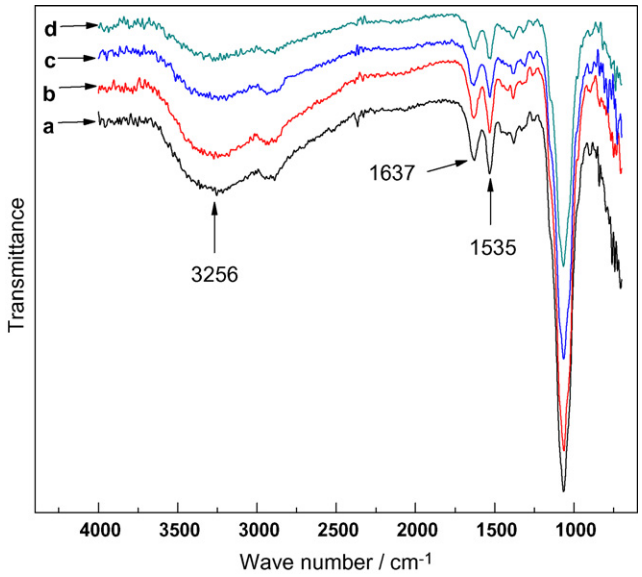


**Fig. 2.** FTIR spectra of CS and nanocomposite membranes: (a) CS, (b) CS/PTNT-5, (c) CS/PTNT-15 and (d) CS/PTNT-25.

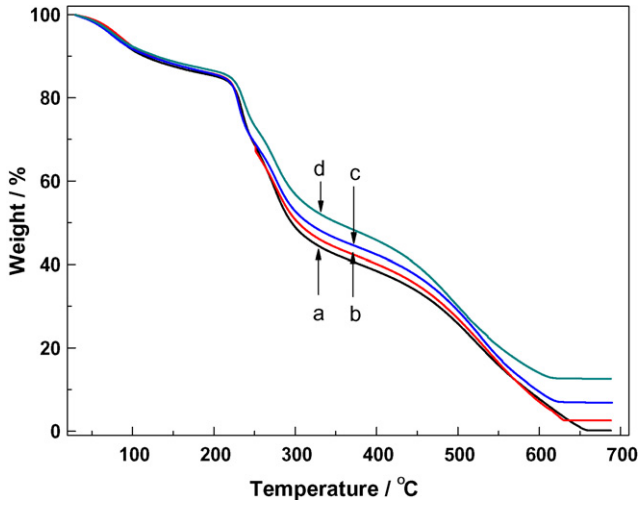


**Fig. 3.** TGA thermodiagram of CS and nanocomposite membranes: (a) CS, (b) CS/PTNT-5, (c) CS/PTNT-15 and (d) CS/PTNT-25.

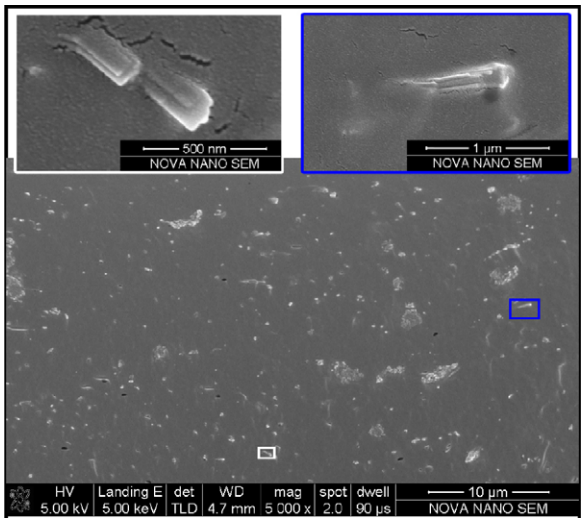


**Fig. 4.** FESEM image of the cross section of the nanocomposite membrane.

worthy that the values of char yields (2.57% for CS/PTNT-5, 6.85% for CS/PTNT-15 and 12.57% for CS/PTNT-25) were almost 60% of the amounts of the PTNTs additives originated from the loss of phosphoric acid groups and adsorbed water. Such phenomena also indicated that the increased char ratios were mainly resulted from the nonvolatile tubes and not from the chitosan matrix. Accordingly, the thermal degradation mechanism of chitosan might not be altered by the embedded additives. Similar results were also reported for other nanocomposite membranes [34]. It should be pointed out that the CS/PTNT membranes were stable at operating temperatures (<100 °C) for DMFC.

Since the transport of methanol within DMFC membrane can be described by solution-diffusion mechanism, in which the process is dominated by the diffusivity of methanol in most cases [35,36], the nanoscale morphology would strongly influence the membrane performance. The internal morphologies of the as-prepared membranes were determined by FESEM and PALS, the results of which are shown in Fig. 4 and Table 1, respectively. FESEM observations of the representative membrane (CS/PTNT-15) demonstrated that the nanotubes still kept the intact tubular structure during the membrane preparation. The nanotubes associated around 100 nm in diameter and dispersed homogeneously in chitosan matrix without obvious agglomeration. It could be seen that the interfacial interactions improved the interfacial compatibility between the nanotubes and polymer matrix, and thus avoiding micro-phase separation as well as non-selective voids at the interface.

**Table 1**
Free volume parameters of the as-prepared membranes.

| Entry | Membrane | $\tau_3$ (ns) | $I_3$ (%) | $r_3$ (nm) | $V_f$ (nm$^3$) | *FFV* (%) |
|---|---|---|---|---|---|---|
| 1 | CS | 2.022 | 16.40 | 0.2868 | 0.0988 | 1.620 |
| 2 | CS/PTNT-H3 | 2.002 | 15.32 | 0.2850 | 0.0969 | 1.485 |
| 3 | CS/PTNT-H2 | 2.015 | 15.26 | 0.2862 | 0.0981 | 1.498 |
| 4 | CS/PTNT-H1 | 2.026 | 15.67 | 0.2872 | 0.0992 | 1.554 |
| 5 | CS/PTNT-H0 | 2.045 | 15.60 | 0.2889 | 0.1010 | 1.575 |
| 6 | CS/PTNT-3 h | 2.010 | 16.02 | 0.2857 | 0.0976 | 1.564 |
| 7 | CS/PTNT-6 h | 1.982 | 15.89 | 0.2832 | 0.0951 | 1.511 |
| 8 | CS/PTNT-9 h | 1.978 | 15.63 | 0.2828 | 0.0947 | 1.480 |
| 9 | CS/PTNT-12 h | 1.962 | 15.71 | 0.2813 | 0.0932 | 1.464 |
| 10 | CS/PTNT-5 | 2.010 | 15.67 | 0.2857 | 0.0976 | 1.530 |
| 11 | CS/PTNT-10 | 2.012 | 15.46 | 0.2859 | 0.0978 | 1.513 |
| 12 | CS/PTNT-15 | 2.009 | 15.41 | 0.2857 | 0.0976 | 1.505 |
| 13 | CS/PTNT-20 | 2.005 | 15.24 | 0.2853 | 0.0972 | 1.482 |
| 14 | CS/PTNT-25 | 2.002 | 15.35 | 0.2850 | 0.0969 | 1.488 |
| 15 | CS/PTNT-30 | 1.970 | 15.13 | 0.2820 | 0.0939 | 1.421 |

Free volume characteristics of the prepared membranes were also investigated to get a deeper understanding of the material microstructure, which were reported as an effective direct datum for describing membrane morphology [37]. PALS technique, as a unique and direct way, was employed to probe the free volume parameters of chitosan and nanocomposite membranes, and the results are tabulated in Table 1. The free volume parameters indicated that pure CS membrane (Entry 1) possessed free volume cavities with an average radius of about 0.287 nm, which was in agreement with the results in the literature [38]. This kind of cavity belonged to network pores (in the range of 0.20–0.30 nm), which meant the small spaces between polymer segments constituting the polymer aggregate [37]. After the PTNTs incorporation, the average radius of the free volume cavity of the membranes reduced ($r_3$ parameter, Entries 2–15). The reduction of radius should be attributed to the strong interactions between the fillers and chitosan chains, which generated stress at the organic–inorganic interface during solution evaporation. The strong stress would inhibit the mobility of polymer chains and hence lead to dense chain packing near the interfacial domains [29,39]. The results of free volume characteristics were in good agreement with the characterization of FTIR and TGA. According to Fujita free volume theory, the fractional free volume would directly determine the diffusivity of the methanol though the membrane [40]. As shown in Table 1, the fractional free volume of the nanocomposite membranes (Entries 2–15) was lower than that of pure CS membrane (Entry 1), which was advantageous to suppress methanol crossover (as discussed hereafter).

### 3.3. Elucidation of the modification conditions upon the membrane performance

#### 3.3.1. Effect of phosphorylation reagent

The effect of phosphorylation reagent on the phosphorylated samples was investigated by FTIR and XPS analysis. It can be clearly seen from the FTIR results as shown in Fig. 5, the intensity of the band that corresponded to P–OH (1045 $cm^{-1}$) followed the order of PTNT-H0 < PTNT-H1 < PTNT-H2 < PTNT-H3, which indicated an increase in the amount of phosphoric acid groups. This could also be confirmed by the XPS characterization: the P atom contents for PTNT-H0, PTNT-H1, PTNT-H2 and PTNT-H3 were 0.9%, 1.1%, 1.5% and 3.6%, respectively. Such phenomena were reasonably ascribed to the enhancing degree of Coulombic interactions between phosphate ions and the TNTs with the decrease of pH value from 13.2 to 1.7, resulting in an obvious increase of the amount of absorbed phosphoric acid on the surface of the nanotubes. Similar phenomena were observed for phosphorylated $TiO_2$ nanoparticles [30,32]. In addition, as phosphoric acid groups increased, the absorption bands at 1635 and 3384 $cm^{-1}$ attributed to the absorbed water increased as shown in Fig. 5b–e.

The membrane performance including water uptake, swelling, methanol permeability, proton conductivity and selectivity of CS, CS/PTNT-H3, CS/PTNT-H2, CS/PTNT-H1, CS/PTNT-H0 and a Nafion 117 membrane is summarized in Table 2. The water uptake in a proton-conducting membrane is an important factor that strongly affects the proton transport. For these composite membranes, the total water uptake mainly consisted of two parts, the first part was the water uptake in bulk polymer depended on its fractional free volume, and the other was the water uptake in tubes determined by the amount of acid groups. Table 2 suggests that the nanocomposite membranes exhibited lower water uptake than pure CS membrane. This observation indicated that the water uptake in bulk polymer contributed more than that in nanotubes to the total water uptake. For nanocomposite membranes, the water uptake decreased (Entries 3–6) with the decrease of phosphoric acid. Such phenomena should be originated from the decrease of water uptake in bulk chitosan but remarkable increase in the fillers, as testified by PALS and FTIR analysis. The swelling of the membrane was mainly caused by the water adsorption in bulk polymer, and hence the addition of PTNTs reduced the swelling of the membrane as a result of the reduction of water uptake in bulk polymer.

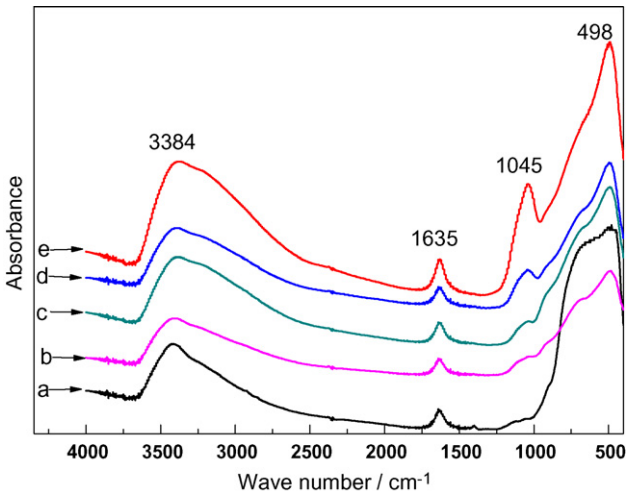


**Fig. 5.** FTIR spectra of TNTs and PTNTs modified by different phosphorylation reagents: (a) TNTs, (b) PTNT-H0, (c) PTNT-H1, (d) PTNT-H2 and (e) PTNT-H3.

The free volume cavities could provide diffusing molecules with a low-resistance path for transport, thus the larger and more numerous free volume elements are, the faster molecules migrate through a membrane [27,28,38]. The methanol crossover of Nafion 117 in 2 M methanol solution was $3.14 \times 10^{-6}$ $cm^2$ $s^{-1}$, which was consistent with the literature [29]. By comparison, CS based membrane displayed excellent methanol barrier property and the methanol crossover was less than 40% of that of Nafion membrane. Since the average free volume cavity radius (about 0.28 nm) of these membranes was larger than the kinetic radius of methanol molecule (0.19 nm), methanol transporting through the membrane would occur in these free volume cavities. For CS/PTNT membranes, the presence of nanotubes within chitosan matrix on the one hand reduced the *FFV* for methanol transport, on the other hand induced a tortuous pathway, both of which enhanced the diffusion resistance for methanol and consequently inhibited the methanol crossover. *FFV* parameter in

**Table 2**
The water uptake, swelling, methanol permeability, proton conductivity and selectivity of Nafion 117, CS, CS/PTNT-H3, CS/PTNT-H2, CS/PTNT-H1 and CS/PTNT-H0 membranes.

| Entry | Membrane | Water uptake (%) | Swelling (%) | Methanol permeability ($10^{-7}$ $cm^2$ $s^{-1}$) | Proton conductivity (S $cm^{-1}$) 20 ± 2 °C | Selectivity ($10^5$ S s $cm^{-3}$) |
|---|---|---|---|---|---|---|
| 1 | Nafion 117 | 30.55 | 37.56 | 31.42 | 0.0696 | 0.221 |
| 2 | CS | 58.24 | 40.07 | 13.51 | 0.0123 | 0.904 |
| 3 | CS/PTNT-H3 | 55.46 | 34.47 | 7.43 | 0.0164 | 2.207 |
| 4 | CS/PTNT-H2 | 51.53 | 34.78 | 7.83 | 0.0140 | 1.788 |
| 5 | CS/PTNT-H1 | 48.22 | 36.4 | 7.92 | 0.0121 | 1.528 |
| 6 | CS/PTNT-H0 | 45.98 | 39.19 | 8.52 | 0.0115 | 1.349 |

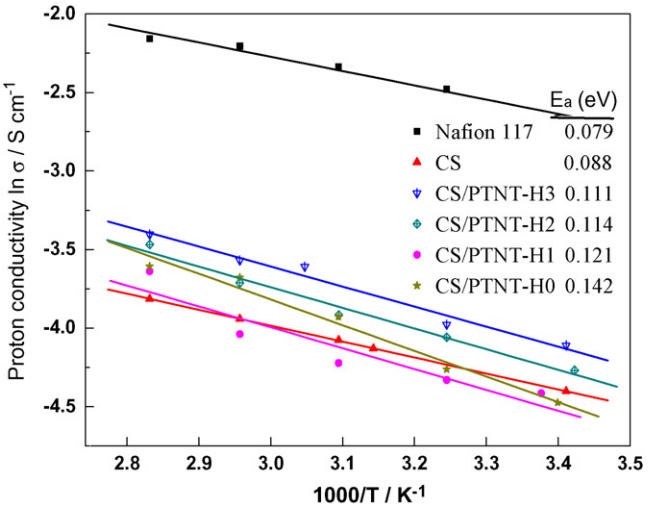


**Fig. 6.** Proton conductivity of CS, CS/PTNT-H3, CS/PTNT-H2, CS/PTNT-H1, CS/PTNT-H0 and a Nafion 117 membrane as a function of temperature at 100% RH.

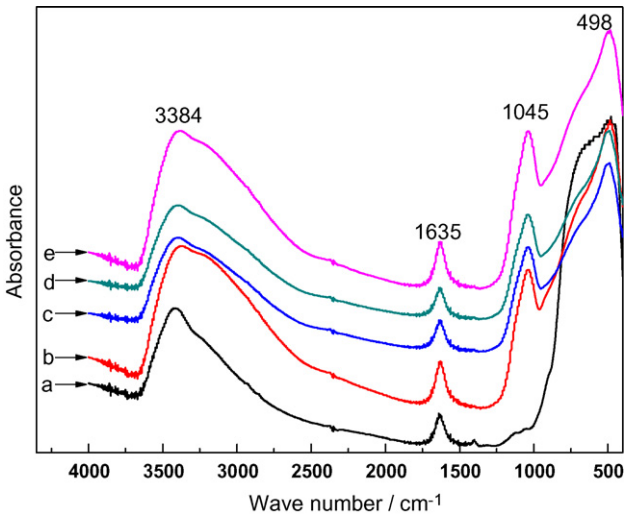


**Fig. 7.** FTIR spectra of TNTs and PTNTs modified with different immersing times: (a) TNTs, (b) PTNT-3 h, (c) PTNT-6 h, (d) PTNT-9 h and (e) PTNT-12 h.

Table 1 revealed that the reducing phosphoric acid groups in fillers resulted in an increasing *FFV* of the composite membranes under a certain filler content. Accordingly, the methanol permeability of PTNTs embedded membranes followed the order of CS/PTNT-H0 > CS/PTNT-H1 > CS/PTNT-H2 > CS/PTNT-H3.

The proton conductivity results listed in Table 2 indicated that pure chitosan membrane exhibited desirable proton conductivity (about 0.012 S cm$^{-1}$) for the application in DMFC (>0.01 S cm$^{-1}$) [41]. To elucidate the effect of phosphorylated nanotubes on proton conductivity of the membrane, equal amounts of phosphoric acid (0.039 g) and TNTs (0.186 g) to CS/PTNT-H3 were separately incorporated into CS membrane. Under the same measuring conditions, the proton conductivity of these two membranes was 0.0142 and 0.0081 S cm$^{-1}$, respectively, which were both lower than that of CS/PTNT-H3 (0.0164 S cm$^{-1}$). Such observations suggested that the incorporation of the phosphorylated nanotubes could immobilize acid groups and construct a continuous proton conductive channel with the aid of P–OH groups and adsorbed water. As a result, an enhancement in proton conductivity of the membrane was observed after embedding PTNTs (Entries 3 and 4). On the other hand, as phosphoric acid groups decreased, the facilitation of PTNTs in proton transport became weaker, and consequently decreased the proton conductivity (from 0.0164 to 0.0115 S cm$^{-1}$) of the nanocomposite membranes.

Further study on the proton conductivity at elevated temperatures up to 80 °C at 100% RH was carried out and the results are presented as Arrhenius plots in Fig. 6. The proton conductivities of all membranes increased with increasing the operation temperatures and agreed with the Arrhenius law. The values of the activation energy ($E_a$) for the samples (shown in Fig. 6) were calculated using the Arrhenius equation $\sigma = \sigma_o \exp(-E_a/kT)$, where $\sigma_o$ is a pre-exponential factor, $k$ is the Boltzmann's constant, and the temperature $T$ is in kelvin. In consistent with the results in the literature [42], the activation energy for Nafion 117 was calculated to be 0.079 eV. The activation energy for CS based membranes was in the range of 0.088–0.142 eV, which was higher than that for Nafion but lower than that for only Grotthuss mechanism (0.150–0.418 eV) [43]. These results implied that both the Grotthuss mechanism (protons hoped from one site to a neighboring one) and vehicle mechanism (protons diffused accompanying water molecules) existed in CS based membranes. Furthermore, it could be seen that an increase in phosphoric acid content resulted in a decrease of activation energy ranging from 0.142 to 0.111 eV for the nanocomposite membranes, which suggested a reduction of proton migration barrier.

The comprehensive performance of the membrane was reflected by selectivity $S$, where $S = \sigma/P$ with the proton conductivity $\sigma$ and methanol permeability $P$ [44]. As shown in Table 2 (selectivity parameter), the CS based membranes exhibited obviously higher selectivity as a result of their excellent methanol impermeable ability and relative high proton conductive property, when compared with Nafion 117. In particular, the selectivity of CS/PTNT-H3 (Entry 3) was about ten times of that of Nafion 117 (Entry 1).

### 3.3.2. *Effect of immersing time*

In order to optimize the comprehensive performance of the membrane, the phosphorylated tubes with different immersing times from 3 to 12 h were prepared in phosphoric acid solution. The amount of phosphoric acid in PTNTs was determined by FTIR and XPS analysis. FTIR spectra (Fig. 7) revealed a slightly increasing intensity of the strong peak at around 1045 cm$^{-1}$ (P–OH group) with the immersing time, which indicated an increasing amount of acid groups in the functionalized tubes. This could be confirmed by the XPS results: the contents of P atom for PTNT-3 h, PTNT-6 h, PTNT-9 h and PTNT-12 h were 3.4%, 3.6%, 3.9% and 4.1%, respectively. Accordingly, the adsorbed water (vibrational fingerprints at 1635 and 3384 cm$^{-1}$) in the PTNTs increased as shown in Fig. 5b–e.

**Table 3**
The water uptake, swelling, methanol permeability, proton conductivity and selectivity of CS, CS/PTNT-3 h, CS/PTNT-6 h, CS/PTNT-9 h and CS/PTNT-12 h membranes.

| Entry | Membrane | Water uptake (%) | Swelling (%) | Methanol permeability ($10^{-7}$ cm$^2$ s$^{-1}$) | Proton conductivity (S cm$^{-1}$) 20 ± 2 °C | Selectivity ($10^5$ S s cm$^{-3}$) |
|---|---|---|---|---|---|---|
| 1 | CS | 58.24 | 40.07 | 13.51 | 0.0123 | 0.904 |
| 2 | CS/PTNT-3 h | 54.11 | 35.71 | 8.64 | 0.0158 | 1.829 |
| 3 | CS/PTNT-6 h | 55.30 | 34.50 | 7.50 | 0.0165 | 2.200 |
| 4 | CS/PTNT-9 h | 55.89 | 33.29 | 6.68 | 0.0168 | 2.515 |
| 5 | CS/PTNT-12 h | 56.90 | 32.66 | 6.42 | 0.0175 | 2.726 |

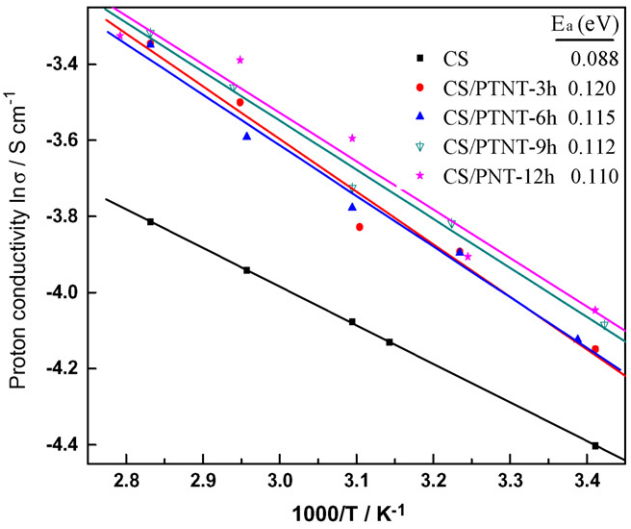


**Fig. 8.** Proton conductivity of CS, CS/PTNT-3 h, CS/PTNT-6 h, CS/PTNT-9 h and CS/PTNT-12 h as a function of temperature at 100% RH.

For the nanocomposite membranes, the fractional free volume decreased from 1.564% for CS/PTNT-3 h to 1.464% for CS/PTNT-12 h (*FFV* parameter in Table 1, Entries 6–9) as phosphoric acid groups increased and the water uptake in bulk chitosan was therefore decreased. This could be confirmed by the reduction (from 35.71% to 32.66%) of the membrane swelling, which was mainly caused by the adsorption of water in polymer phase. On the other hand, the increasing acid groups in PTNT resulted in an enhancing water uptake within the nanotubes, as testified by FTIR results. The total water uptake of the membranes consisting of these two sections was therefore changed only slightly by less than 5.2% (water uptake parameter in Table 3, Entries 2–5).

The methanol permeability listed in Table 3 suggested a significant enhancement of methanol barrier property (Entries 2–5) after embedding PTNTs into chitosan matrix. For the nanocomposite membranes, the PALS characterization revealed a reduction in both average free volume cavity radius (from 0.2857 nm for CS/PTNT-3 h to 0.2813 nm for CS/PTNT-12 h) and fractional free volume (from 1.564% to 1.464%) with the acid groups, both of which increased the diffusion resistance for methanol molecules. The methanol crossover of the membrane was consequently reduced from $8.64 \times 10^{-7}$ to $6.42 \times 10^{-7}$ cm$^2$ s$^{-1}$.

Proton conductivity results indicated that the addition of the phosphorylated fillers into chitosan membrane obviously improved the proton conductivity from 0.0123 to 0.0158 S cm$^{-1}$ at $20 \pm 2$ °C. FTIR and XPS analysis revealed an increase of phosphoric acid groups and absorbed water in nanotubes with immersing time. Both of these would facilitate the proton transport through the uninterrupted channels constructed by the nanotubes, and consequently improved the proton conductivity from 0.0158 to 0.0175 S cm$^{-1}$. Fig. 8 illustrates the temperature dependence of proton conductivity of these membranes at 100% RH as Arrhenius plots. The calculated activation energy for the membranes was in the range of 0.088–0.120 eV. Accordingly, the proton transfer through these membranes was in the view of Grotthuss mechanism and vehicle mechanism. For the nanocomposite membrane, the increasing acid groups would induce a decreasing resistance for proton transfer within the channels, and thus reduced the activation energy (from 0.12 to 0.11 eV).

Selectivity results presented in Table 3 suggested an obvious enhancement of comprehensive performance after PTNTs incorporation. For nanocomposite membranes (Entries 2–5), the comprehensive performance improved from $1.829 \times 10^5$ S s cm$^{-3}$ for CS/PTNT-3 h to $2.726 \times 10^5$ S s cm$^{-3}$ for CS/PTNT-12 h owing to their enhanced methanol impermeable and proton conductive properties. It should be pointed out that titanate nanotubes were unstable in acid solution as a result of a neutralization reaction, and the tubular structure would be destructed slowly to granular structure [45]. Therefore, the treatment time of titanate nanotubes by phosphoric acid was limited to avoid their structure destruction.

### 3.4. Effect of PTNTs content upon membrane performance

The influence of PTNTs content on the membrane performance was also evaluated and the results are presented in Table 4. Since water uptake in bulk chitosan was higher than that in the tubes as mentioned above, a reduction in water uptake of the membrane was observed after the addition of nanotubes, and it decreased further from 56.68% to 43.16% with the increase of filler content from 5% to 30% for nanocomposite membranes. As a result, the swelling of the membranes decreased from 38.73% for CS/PTNT-5 to 28.80% for CS/PTNT-30.

Methanol permeability test implied decreased methanol crossover of the membrane by embedding phosphorylated nanotubes, as shown in Table 4. As the filler content increased from 5% to 30%, the methanol crossover reduced from $8.93 \times 10^{-7}$ to $6.87 \times 10^{-7}$ cm$^2$ s$^{-1}$, which was possibly originated from the decreasing fractional free volume as well as the lengthening methanol pathway.

The proton conductivity of the membranes summarized in Table 4 and Fig. 9 revealed that the nanocomposite membranes (Entries 2–7) displayed higher proton conductivities compared with pure CS membrane (Entry 1). Meanwhile, the proton conductivity improved from 0.0128 to 0.0202 S cm$^{-1}$ with the filler content at $20 \pm 2$ °C. The observations indicated that more continue channels with high proton conductive ability were formed within the nanocomposite membranes for protons transfer. Fig. 9 shows that all the membranes exhibited increasing proton conductivity with the temperature at 100% RH. Previous studies found that the proton conduction mechanism of phosphorylated materials was predominant in the view of Grotthuss mechanism rather than vehicle mechanism [46]. Accordingly, as the filler content increased, more protons would transport according to Grotthuss mechanism via the constructed pathway, and this mechanism became predominant in the nanocomposite membranes. The activation energy of

**Table 4**
The water uptake, swelling, methanol permeability, proton conductivity and selectivity of CS and CS/PTNT-*X* membranes.

| Entry | Membrane | Water uptake (%) | Swelling (%) | Methanol permeability ($10^{-7}$ cm$^2$ s$^{-1}$) | Proton conductivity (S cm$^{-1}$) at $20 \pm 2$ °C | Selectivity ($10^5$ S s cm$^{-3}$) |
|---|---|---|---|---|---|---|
| 1 | CS | 58.24 | 40.07 | 13.51 | 0.0123 | 0.904 |
| 2 | CS/PTNT-5 | 56.68 | 38.73 | 8.93 | 0.0128 | 1.433 |
| 3 | CS/PTNT-10 | 53.42 | 34.30 | 8.26 | 0.0150 | 1.816 |
| 4 | CS/PTNT-15 | 48.12 | 33.27 | 7.48 | 0.0164 | 2.193 |
| 5 | CS/PTNT-20 | 46.73 | 31.42 | 7.26 | 0.0173 | 2.383 |
| 6 | CS/PTNT-25 | 45.65 | 29.52 | 6.98 | 0.0182 | 2.607 |
| 7 | CS/PTNT-30 | 43.16 | 28.80 | 6.87 | 0.0202 | 2.940 |

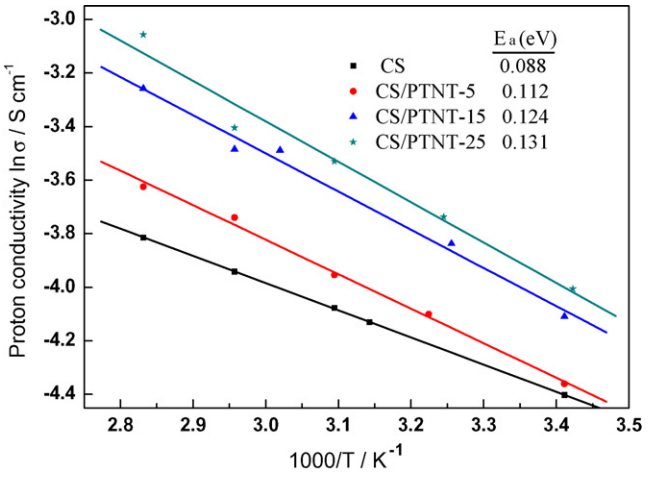


**Fig. 9.** Proton conductivity of CS, CS/PTNT-5, CS/PTNT-15 and CS/PTNT-25 as a function of temperature at 100% RH.

the membrane (shown in Fig. 9) was therefore increased close to the $E_a$ for Grotthuss mechanism (0.150–0.418 eV). Similar observations were reported for other organic–inorganic composite membrane [47,48].

According to the selectivity parameter in Table 4, the comprehensive performance of the membranes improved with the increase of filler content as a result of the enhancing methanol barrier and proton conductive properties. In particular, the selectivity of the nanocomposite membranes improved by 50% from $1.43 \times 10^5$ to $2.94 \times 10^5$ S s cm$^{-3}$ as the filler content increased from 5% to 30%.

## 4. Conclusions

A series of nanocomposite membranes were fabricated by embedding phosphorylated titanate nanotubes of varying phosphoric acid contents into chitosan matrix. The incorporation of phosphorylated nanotubes played the dual roles in enhancing the membrane performances: (1) suppressing the methanol crossover by reducing the fractional free volume of the membrane due to strong interfacial interactions and (2) facilitating the proton transfer by constructing continue conductive channels with the aid of P–OH groups and adsorbed water molecules. By prolonging the treatment time or decreasing the pH value of the phosphorylation reagent, the phosphoric acid groups in the functionalized tubes increased obviously. For nanocomposite membranes, the increasing acid groups of PTNTs would further decrease their *FFV*, and therefore, an improved methanol barrier property was acquired. Meanwhile, the increasing acid groups would facilitate the proton transport through the membranes as testified by the decreased activation energy for proton transfer, and thus resulting in enhanced proton conductivity. Furthermore, the enhancement of membrane performances became greater with the increase of PTNTs content. In particular, the incorporation of 30% PTNT-6 h simultaneously reduced the methanol crossover by 50% and increased the proton conductivity by 64% in comparison with the plain CS membrane.

## Acknowledgements

We gratefully acknowledge financial support from the National Nature Science Foundation of China (No. 20776101), the Programme of Introducing Talents of Discipline to Universities (No. B06006) and the Program for Changjiang Scholars and Innovative Research Team in University from the Ministry of Education of China.

## References

[1] K. Vinodgopal, M. Haria, D. Meisel, P. Kamat, Nano Lett. 4 (2004) 415–418.
[2] Y.L. Hsin, K.C. Hwang, C.T. Yeh, J. Am. Chem. Soc. 129 (2007) 9999–10010.
[3] T. Yamaguchi, H. Zhou, S. Nakazawa, N. Hara, Adv. Mater. 19 (2007) 592–596.
[4] K. Schmidt-Rohr, Q. Chen, Nat. Mater. 7 (2008) 75–83.
[5] K.D. Kreuer, S.J. Paddison, E. Spohr, M. Schuster, Chem. Rev. 104 (2004) 4637–4678.
[6] S.P. Jiang, Z. Liu, Z.Q. Tian, Adv. Mater. 18 (2006) 1068–1072.
[7] Y.F. Lin, C.Y. Yen, C.H. Hung, Y.H. Hsiao, C.C.M. Ma, J. Power Sources 168 (2007) 162–166.
[8] K.D. Kreuer, Chem. Mater. 8 (1996) 610–641.
[9] J.D. Kim, T. Mori, I. Honma, J. Electrochem. Soc. 153 (2006) A508–A514.
[10] S.R. Narayanan, S.P. Yen, L. Liu, S.G. Greenbaum, J. Phys. Chem. B 110 (2006) 3942–3948.
[11] W.F. Chen, J.S. Wu, P.L. Kuo, Chem. Mater. 20 (2008) 5756–5767.
[12] J.M. Thomassin, J. Kollar, G. Caldarella, A. Germain, R. Jérome, C. Detrembleur, J. Membr. Sci. 303 (2007) 252–257.
[13] S.H. Joo, C. Pak, E.A. Kim, Y.H. Lee, H. Chang, D. Seung, Y.S. Choi, J.B. Park, T.K. Kim, J. Power Sources 180 (2008) 63–70.
[14] S.J. Paddison, K.D. Kreuer, J. Maier, Phys. Chem. Chem. Phys. 8 (2006) 4530–4542.
[15] M. Schuster, T. Rager, A. Noda, K.D. Kreuer, J. Maier, Fuel Cells 5 (2005) 355–365.
[16] J. Weber, K.D. Kreuer, J. Maier, A. Thomas, Adv. Mater. 20 (2008) 2595–2598.
[17] Q.F. Li, H.A. Hjuler, N.J. Bjerrum, J. Appl. Electrochem. 31 (2001) 773–779.
[18] A.L. Rusanov1, P.V. Kostoglodov, M.J.M. Abadie, V.Y. Voytekunas, D.Y. Likhachev, Adv. Polym. Sci. 216 (2008) 125–155.
[19] M.Y. Jang, Y. Yamazaki, J. Power Sources 139 (2005) 2–8.
[20] M.L. Hill, Y.S. Kim, B.R. Einsla, J.E. McGrath, J. Membr. Sci. 283 (2006) 102–108.
[21] F. Bauer, M. Willert-Porada, J. Power Sources 145 (2005) 101–107.
[22] G. Alberti, U. Costantino, M. Casciola, S. Ferroni, L. Massinelli, P. Staiti, Solid State Ionics 145 (2001) 249–255.
[23] G.L. Athens, Y. Ein-Eli, B.F. Chmelka, Adv. Mater. 19 (2007) 2580–2587.
[24] J. Geng, Z. Jiang, Y. Wang, D. Yang, Scripta Mater. 59 (2008) 352–355.
[25] Y.J. Weng, R.X. Hou, G.C. Li, J. Wang, N. Huang, H.Q. Liu, Appl. Surf. Sci. 254 (2008) 2712–2719.
[26] L. Krsi, S. Papp, I. Bertti, I. Dkny, Chem. Mater. 19 (2007) 4811–4819.
[27] P. Winberg, K. DeSitter, C. Dotremont, S. Mullens, I.F.J. Vankelecom, F.H.J. Maurer, Macromolecules 38 (2005) 3776–3782.
[28] M. García, J. Barsema, R.E. Galindo, D. Cangialosi, J. Garcia-Turiel, W.E. Van Zyl, H. Verweij, D.H.A. Blank, Polym. Eng. Sci. 44 (2004) 1240–1246.
[29] J. Wang, H. Zhang, Z. Jiang, X. Yang, L. Xiao, J. Power Sources 188 (2009) 64–74.
[30] H.P. Wu, T.L. Cheng, W.L. Tseng, Langmuir 23 (2007) 7880–7885.
[31] D. Zhao, C. Chen, Y. Wang, H. Ji, W. Ma, L. Zang, J. Zhao, J. Phys. Chem. C 112 (2008) 5993–6001.
[32] P.A. Connor, A.J. McQuillan, Langmuir 15 (1999) 2916–2921.
[33] Y.L. Liu, C.Y. Hsu, Y.H. Su, J.Y. Lai, Biomacromolecules 6 (2005) 368–373.
[34] T. Kashiwagi, A.B. Morgan, J.M. Antonucci, M.R. VanLandingham, R.H. Harris Jr., W.H. Awad, J.R. Shields, J. Appl. Polym. Sci. 89 (2003) 2072–2078.
[35] N. Miyake, J.S. Wainright, R.F. Savinell, J. Electrochem. Soc. 148 (2001) A905–A909.
[36] Z.X. Liang, T.S. Zhao, J. Prabhuram, J. Membr. Sci. 283 (2006) 219–224.
[37] S.H. Kim, S.Y. Kwak, T. Suzuki, Environ. Sci. Technol. 39 (2005) 1764–1770.
[38] J. Wang, X. Zheng, H. Wu, B. Zheng, Z. Jiang, X. Hao, B. Wang, J. Power Sources 178 (2008) 9–19.
[39] T.T. Moore, W.J. Koros, J. Mol. Struct. 739 (2005) 87–98.
[40] H. Fujita, Fortschr. Hochpolym. Forsch. 3 (1961) 1–47.
[41] V. Neburchilov, J. Martin, H. Wang, J. Zhang, J. Power Sources 169 (2007) 221–238.
[42] E. Cho, J.S. Park, S.S. Sekhon, G.G. Park, T.H. Yang, W.Y. Lee, C.S. Kim, S.B. Park, J. Electrochem. Soc. 156 (2009) B197–B202.
[43] Y. Jin, S. Qiao, J.C. Diniz da Costa, B.J. Wood, B.P. Ladewig, G.Q. Lu, Adv. Funct. Mater. 17 (2007) 3304–3311.
[44] D.K. Kim, G.P. Robertson, M.D. Guiver, Macromolecules 41 (2008) 2126–2134.
[45] D.V. Bavykin, J.M. Friedrich, A.A. Lapkin, F.C. Walsh, Chem. Mater. 18 (2006) 1124–1129.
[46] S.Ü. Celik, A. Aslan, A. Bozkurt, Solid State Ionics 179 (2008) 683–688.
[47] M.L. Di Vona, D. Marani, A. D'Epifanio, S. Licoccia, I. Beurroies, R. Denoyel, P. Knauth, J. Membr. Sci. 304 (2007) 76–81.
[48] V.K. Shahi, Solid State Ionics 177 (2007) 3395–3404.